Contents

10. Prediction of Large Negative Shaded-Side Spacecraft Potentials

S. M. L. Prokopenko and J. G. Laframboise
Physics Department
York University
Toronto, Canada

Abstract

A calculation by Knott, for the floating potential of a spherically symmetric synchronous-altitude satellite in eclipse, has been adapted to provide simple calculations of upper bounds on negative potentials which may be achieved by electrically isolated shaded surfaces on spacecraft in sunlight. To investigate geometrical effects, we have replaced Knott's use of the orbit-limited ion current expression for a sphere, by that for an infinite cylinder. Large (~60 percent) increases in predicted negative shaded-side potentials are obtained as a result. To investigate "effective-potential barrier" or "angular-momentum selection" effects due to the presence of less-negative sunlit-side or adjacent-surface potentials, we have also replaced these expressions by the ion random current, which is a lower bound for convex surfaces when such effects become very severe. Further large increases in predicted negative potentials are obtained, amounting to a doubling in some cases. Depending on surface properties and incident energy distributions, values exceeding -20 kV are now predicted, in good agreement with ATS-6 observations of potentials reaching -19 kV, as reported by Whipple. For isolated surfaces in shaded cavities, even more negative values may be reached. In some conditions, two distinct floating potentials exist, leading to the possibility of "bifurcation phenomena" in real situations.

I. INTRODUCTION

The performance of many satellites in synchronous orbit has been degraded by anomalous events which include frequent spurious spacecraft commands and in some cases permanent damage. These events invariably appear to involve electrical discharges caused by differential charging of spacecraft surfaces to large relative potentials. The latter condition in turn is known to result from the relatively large average energies (up to a few keV) of the charged particle environment at synchronous orbit altitude, particularly in disturbed magnetospheric conditions. Since photoelectron emission from sunlit surfaces tends to compensate for incident electron fluxes, thereby holding sunlit-side surface potentials close to space potential in most cases, an estimate of differential charging magnitudes can be obtained by simply calculating floating potentials of electrically isolated shaded surfaces, relative to space potential. In the present work, we have attempted to obtain upper bounds on such potentials, which in cases of interest are usually highly negative, because these bounds constitute "worst cases" for design purposes, and also because unlike more exact calculations, they can be obtained from simple current balance calculations. Furthermore, it is sufficient to consider local current balance only, because this corresponds to an electrically isolated surface element, which is also a "worst case" for differential charging. To calculate these bounds, we have extended a calculation by Knott,[1] of the floating potential of a spherically symmetric synchronous-altitude satellite in eclipse. To investigate geometrical effects, we have replaced Knott's use of the Mutt-Smith and Langmuir[2] orbit-limited current expression for collection of Maxwellian ions by a unipotential sphere, by the corresponding expression for an infinite cylinder; both expressions have been shown[3] to be upper bounds for collisionless ion collection as a function of local surface potential, for three- and two-dimensional collectors, respectively, regardless of collector shape, sheath potential, or potential of other parts of the collector. This replacement causes a large decrease in ion collection and a correspondingly large increase in negative shaded-side floating potentials (Section 3). Another important ion-current restriction may be caused by "effective-potential barrier"[3,4,5] or "angular-momentum selection" effects, in which the presence of less-negative sunlit-side potentials produces dipole and higher moments in the sheath potential,[6] causing steepening and contraction of the potential well surrounding the shaded side (Figure 1). A similar steepening effect will also occur if an isolated shaded surface element is surrounded by adjacent shaded surfaces which for any reason have less negative potentials (Figure 2). The most extreme possibility would be a potential profile which was equal to space potential almost to the spacecraft surface, then fell discontinuously to surface potential. This limit would correspond to a "planar sheath" situation in which the ion collection

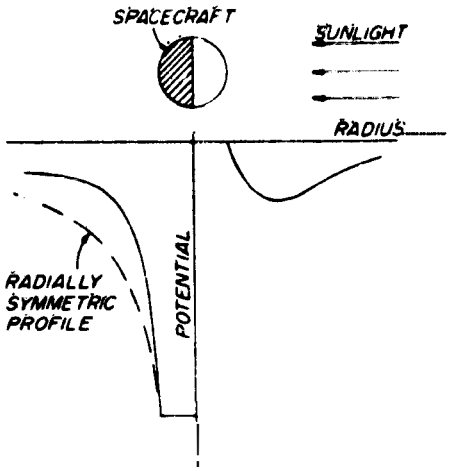

Figure 1. Steepening of Shaded Side Potential Profile for a Spacecraft with an Insulated Surface, after Fahleson[6]

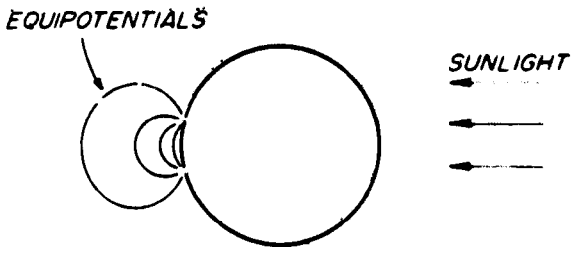

Figure 2. Conductive Spacecraft with Shaded Isolated Surface Patch

on any shaded convex sufface **would** be given by **just** the ion random flux. This amouhts to a further ion current restriction which produces even **larger** increases in negative shaded-side floating potentials (Section 3). This situation correspohds to a velocity-space cutoff boundary for incident ions which is "one-dimehsional;" the cutoff bouridaries corresponding to spherical and infinite cylindrical collectors **are,** respectively, "three-dimensional" and "two-dimenstional"[3] (Section 2).

We also shbw (Section 3) that if shaded cavities containing isolated surfaces exist on a spacecraft, negative pbtentials on such surfaced may surpass **even** these predictions. In some cases, more than one possible floating potential results fram the calculatiun; this implies the possibility of "bifurcation phenomena" in which adjacent isolated surfaces of the same material may arrive at different floating potentials as a result of differences in their charging histories (Section 3).

We have also modified Knott's calculation in another way, by including currents due **to** electron backscattering (Section 2). These currents will tend to decrease net electron collection, thereby making floating potentials less negative thah otherwise (Section 3). **A** process not included **by** either Knott or ourselves is secondary electron emission due to Ion impacts; this will also tend **to** make floating potentials less negative.

2. THEORY

The ambient electron energy distributions used in the present work are a model quiet-time spectrum (Knott,[1] Figure 1) and a model disturbed spectrum (Knott,[1] Figure 2b) based on measurement3 by Shield and Prank,[7] and DeForest and McIlwain,[8] respectively. Both of these distributions, and also the ambient ion distribution, are assumed isotropic. The disturbed spectrum was chosen from the three ueed by Knott because it has a higher average electron energy (~10 keV) than the others. In using it, we have changed it as follows: in the energy ranger 0.5 keV $\leq E \leq$ 16 keV arid 10 keV $\leq E \leq$ 40 keV, we have replaced Knott's differential energy spectrum by $\sqrt{2} \times 10^8 E^{-1/2}$ and $\sqrt{2} \times 10^9 E^{-3/2}$ electrons/cm^2 sec sr keV, respectively, where E is energy. These r-' .ions are simpler than those indicated by Knott, and they also bring the model spectrum into closer agreement With the data on which it is based. We therefore believe that they may have been the ones actually used by Knott, and that the corresponding parts of Figure 2b in his paper may be incorrectly plotted. For any spatecraft surface having a negative potential $\phi_s < 6$, or for a three-dimensional (for example, spherical) surface having $\phi_s > 6$, the orbit-limited flux (particle current density) J_e of ambient electrons is given by:[3]

$$J_e = \int f v_n \, d^3\underline{v} = \int_{\max(0, -e\phi_s)}^{\infty} (1 + e\phi_s/E)(dJ_{eo}/dE)\, dE \qquad (1)$$

where e is magnitude of unit electronic charge, ϕ_s is local surface potential, dJ_{eo}/dE is the ambient energy-differential flux inciderit on one side of an arbitrarily oriented surface element, and v_n is the velocity component normal to thr same surface element. dJ_{eo}/dE is π times the energy-differeritial flux per steradian used by Knott,[1] and is given in terms of the ambient electron velocity distribution $f \cdot d^3N_\infty/d^3\underline{v}$ By the relation $dJ_{eo}/dE = 2\pi f E/m_e^2$, where m_e is electron mass and N_∞ is ambient ion or electron number density. Since f is isotropic, $f = f(E)$. The factor $(1 + e\phi_s/E)$ in Eq. (1) appears to have been neglected by Knott, and may account for some minor discrepancies between his results and ours (Section 3). The presence of this factor leads to a divergent integration in Eq. (1) if $\phi_s > 0$, unless $dJ_{eo}/dE \to 0$ as $E \to 0$, that is, f(E) remains finite as $E \to 0$. This implies that the differential fluxes ih Knott's Figures 1-3 must approach zero linearly with E at E values smaller than those shown in these figures. In tho present work we have instead used a less-realistic sharp cutoff at 1 eV; this may slightly affect our results for positive floetirig potentials in Section 3. We have also introduced a sharp upper cutoff at 50 keV in the quiet-time spectrum, also in order to avoid a

divergent integration when calculating average energy for use in backscattering calculations (see below).

In order to obtain the orbit-limited electron flux expression for an arbitrary cylindrical collector, the lower integration limit in Eq. (1) must be replaced by the two-dimensional velocity-space cutoff boundary $E = \max(0, -e\phi_s)$, where E is the total energy of transverse motion $\frac{1}{2} m_e(v_x^2 + v_y^2) - e\phi$, and we have chosen a z coordinate perpendicular to the cylinder cross-section. If $\phi_s > 0$, this complicates the integration in Eq. (1), which may then be done in either of two ways. The first [Laframboise and Parker,[3] Eq. (6)] is to convert Eq. (1) into an integration using cylindrical caordinates in velocity spacc. This method has the disadvantage that the velocity distribution must be integrated over v_z in order to convert it into a distribution of transverse velocities. An alternate method[2, 9] is as follows. We choose rectangular coordinated (v_n, v_t, v_z) in velocity space, such that v_n is the Velocity component in the inward normal direction at the collector surface. The v_t and v_z become tangential coordinates, with v_t in the plane of the cylinder cross-section. We then transform to spherical coordinates (v, θ, ψ) With v_z as polar axis. Then: $v_z = v\cos\theta$, $v_n = v\sin\theta\cos\psi$, and $v_t = v\sin\theta\sin\psi$. For $\phi_s > 0$, Eq. (1) is then replaced by:

$$J_e = \int f v_n d^3\underline{v}$$

$$= 2\int_{E=0}^{E=\infty}\int_{\psi=-\pi/2}^{\psi=\pi/2}\int_{\theta=\mathrm{Arc}\sin[e\phi_s/(E+e\phi_s)]^{1/2}}^{\theta=\pi/2} f(E)(v\sin\theta\cos\psi) \times (v^2\sin\theta\, dv\, d\theta\, d\psi)$$

$$= \int_0^\infty \frac{2}{\pi}\left[\mathrm{Arc}\sin\left(\frac{E}{E+e\phi_s}\right)^{1/2} + \frac{(Ee\phi_s)^{1/2}}{E+e\phi_s}\right]\left(1+\frac{e\phi_s}{E}\right)\frac{dJ_{co}}{dE}\,dE \quad . \quad (2)$$

In comparison with Eq. (1), we see that the integrand in Eq. (2) contains an extra, energy-dependent weighting factor, which arises from integration of v_n over the fractional solid angle over whbh ambient electrons can reach the collector at each energy.

A similar procedure is advantageous in obtaining the one-dimensional (Section 1) orbit-limited flux expression. In this case, the lower limit in Eq. (1) must be replaced by: $E_n = \max(0, -e\phi_s)$, where $E_n = \frac{1}{2} m_e v_n^2 - e\phi$. This time

we transform (v_n, v_t, v_z) to spherical coordinates (v, θ, ψ) with v_n as polar axis. For $\phi_s > 0$, Eq. (1) is now replaced by:

$$J_e = \int_{E=0}^{E=\infty} \int_{\theta=0}^{\theta=\text{Arc cos}[e\phi_s/(E+e\phi_s)]^{1/2}} f(E)(v\cos\theta)(2\pi v^2 \sin\theta\, dv\, d\theta)$$

$$= \int_0^\infty \frac{dJ_{eo}}{dE}\, dE \qquad (3)$$

independently of collector potential, as expected.

The correspdndlng expressions for ion flux J_i are simpler because the ions... are assumed to be Maxwellian. Corresponding td the three-, two-, and one-dimensional velocity-space cutoffs described above, we obtain, respectively, *,[3] for–ibn–attracting surface potentials $\chi_{is} > 0$:

$$J_i = J_{io} \begin{cases} (1 + \chi_{is}) & (4) \\ [2(\chi_{is}/\pi)^{1/2} + \exp(\chi_{is})\ \text{erfc}\ (\chi_{is}^{1/2})] & (5) \\ (1) & (6) \end{cases}$$

where $\chi_{is} = -e\phi_s/kT_i$, k is Boltzmann's constant, T_i is ion temperature and J_{io} is the ion random flux $N_\infty(kT_i/2\pi m_i)^{1/2}$. For ion-retarding surface potentials $\chi_{is} < 0$, we obtain:

$$J_i = J_{io} \exp(\chi_{is}) \quad . \qquad (7)$$

We have assumed[1] that T_i = 1 keV, and that the random ion to electron flux ratfo J_{io}/J_{eo} = 0.025.

For the secondary electron fractional yield $\delta(E)$, we have used, following Knott,[1] the relation of Sternglass:[10]

$$\delta(E) = 7.4\, \delta_{max}(E/E_{max}) \exp\,[-2(E/E_{max})^{1/2}] \quad . \qquad (8)$$

We have used the same selection of surface materials (Section 3) as that appearing In Table 1 of Knott,[1] for whkh the values of δ_{max} and E_{max} were obtatned from Gibbons[11] and Hachenberg and Brauer.[12]

The process of electron backscattering, which was not included in Knott's calculations, becomes important at incident electron kinetic energies larger than

those for which secondary emission is dominant. For the backscattered electron fractional yield η, we have fitted the results of Sternglass[13] with a relation of the form:

$$\eta(E) = AE + BE^{1/2} + C \tag{9}$$

where the coefficients A, B, and C are functions of the atomic number Z of the surface material. We have evaluated A, B, and C for each surface material considered (Section 3) by substituting Sternglass' values of η at 1, 3, and 5 keV, into Eq. (9). In all cases, η is a very slowly varying function of E. For compound surface materials, we have assumed that each atomic constituent contributes an independent backscattered flux proportional to its relative concentration. There exist more recent measurements of η[14, 15] which give generally larger values than those of Sternglass,[13] especially for electrons having near-tangential incidence. However, we have found these results to be too fragmentary for our purposes, and we have therefore used Sternglass' results throhghout. Presumably we have therefore underestimated η, and our predicted floating potentials in Section 3 will therefore be slightly more negative than more realistic corresponding values.

When $\phi_s > 0$, not all secondary and backscattered electrons will escape. To calculate Mux escaping, we assume[13], for ease of calculation, that both secondary and backscattered electrons are emitted with Maxwellian velocity distributions hatting thermal energies

$$E_{sec} = kT_{sec} = 1 \text{ ev, and } E_{scat} = kT_{scat} = (0.45 + 2 \times 10^{-3} Z)\overline{E} \text{ eV} ,$$

respectively, regardless of the form of the incident velocity distribution. Here, $\overline{E}$ is the average incident electron energy. We further assume that escape of emitted electrorls is orbit-limited, that is, that no barriers of effective potential[3, 4], or negative barriers of electric potential exist on the shaded aide. Fahleson6 has pointed out that such barriers are likely tu exist on the sunlit side independently of any space-charge effects, if substantial shaded-sunlit differences exist in ϕ_s. The expressions for the escaping secondary and backscattered fluxes J_{sec} arid J_{scat} therefore are:

$$J_{sec} = \int_{-e\phi_s}^{\infty} \delta(E + e\phi_s)(1 + e\phi_s/E)(dJ_{eo}/dE) \tag{10}$$

$$J_{scat} = \int_{-e\phi_s}^{\infty} \eta(E + e\phi_s)(1 + e\phi_s/E)(dJ_{eo}/dE)\, dE \qquad (11)$$

if $\phi_s < 0$. If $\phi_s > 0$, the three-, two-, end one-dimensional cases must ha consid-ered separately. We define $\chi_{sec} \equiv e\phi_s/kT_{sec}$ and $\chi_{scat} \equiv e\phi_s/kT_{scat}$. For brevity, we consider only the secondary fluxes; th& corresponding results for backscattered huxes may be obtained by replacing 6 by η and χ_{sec} by χ_{scat} throughout. If J_s is the emttted flux of secondaries, then thetr velocity distribution at the surface is $f_s = (J_s/2\pi)(m_e/kT_{sec})^2 \exp(-\frac{1}{2} m_e v^2/kT_{sec})$. In the three-dimensional case, the cutoff condition for their escape is $E = \frac{1}{2} m_e v^2 - e\phi_s > 0$. We redefine v_n as velocity component in the outward normal direction, and we use spherical coord-inates as defined in connection with Eq. (3). We obtain, for the escaping secondary flux:

$$J_{sec} = \int f_s\, v_n\, d^3\underline{v}$$

$$= \frac{J_s}{2\pi}\left(\frac{m_e}{kT}\right)^2 \int_{E=0}^{E=\infty} \int_{\theta=0}^{\theta=\frac{\pi}{2}} \exp(-\tfrac{1}{2} m_e v^2/kT_{sec})(v\cos\theta)(2\pi v^2 \sin\theta\, dv\, d\theta)$$

$$= (1 + \chi_{sec}) \exp(-\chi_{sec}) \int_0^{\infty} \delta(E + e\phi_s)(1 + e\phi_s/E)(dJ_{eo}/dE)\, dE \quad . \qquad (12)$$

The factor $(1 + \chi_{sec})$ is noteworthy, because it is specific to three-dimensional, as opposed to planar, sheath geometry. In the two-dimenstonal case, the cutoff condition for excape is $\frac{1}{2} m_e(v_n^2 + v_t^2) - e\phi_s > 0$, and the convolution integral for J_s contains the extra weighting factor which appears in Eq. (2). It is convenient to use spherical coordinates as defined in connection with Eq. (2). We obtaih:

$$J_{sec} = \left[2(\chi_{sec}/\pi)^{1/2} + \exp(\chi_{sec})\, erfc\,(\chi_{sec}^{1/2}) \right] \exp(-\chi_{sec})$$

$$\times \int_0^\infty \frac{2}{\pi} \left[\text{Arc sin} \left(\frac{E}{E + e\phi_s} \right) + \frac{(Ee\phi_s)^{1/2}}{E + e\phi_s} \right] \left(1 + \frac{e\phi_s}{E} \right) \delta(E + e\phi_s)$$

$$\times \frac{dJ_{eo}}{dE}\, dE \quad . \tag{13}$$

In the one-dimensional case, the escape condition is $\frac{1}{2} m_e v_n^2 - e\phi s > 0$, and we again use spherical coordinates as defined in connection with Eq. (3). We obtain:

$$J_{sec} = \exp(-\chi_{sec}) \int_0^\infty \delta(E + e\phi_s)(dJ_{eo}/dE)\, dE \quad . \tag{14}$$

The floating potential(s) of an isolated shaded surface element is (arc) now given by the zero(s) of the function:

$$J_{net} = J_i - J_e + J_{sec} + J_{scat} \quad . \tag{15}$$

3. RESULTS AND DISCUSSION

Table 1 shows floating pbtenttal values obtained by numerical solution of the equation $J_{net} = 0$, where J_{net} is gtven by Eq. (15) and we have assumed $J_{scat} = 0$ in order to duplicate the physical situatibn of Knott,[1] whose results are shown in parentheses. We see that our results show qualitative but not quantitative agreement wtth his. Possible reasons for the disagreement are: (1) Knott appears to have salved the current balance equation graphically rather than numerically; (2) wherever his solution indicates a floating pbtential more negative than -3000 V, he has listed the result simply as "< -3000 V"; (3) wherever he has obtained a positive floating potential, he has listed it simply as "+5 V" whereas we have calculated it using the assumptions made in Section 2; (4) as mentioned following Eq. (1), hls expression for tncident electron flux may contain an error, The most important Feature of Table 1 is the very large floating potentials which are evident in disturbed conditions in the presence of the two- and one-dimensional veloeity-space cutoffs. The dramatic differences which exist among these results are

Table 1. Floating Potentials of Shaded Surfaces of Synchronous-Altitude Spacecraft, Using the Same Surface Properties and Incident Spectra as Assumed by Knott,[1] with Three-, Two-, and One-Dimensional Velocity Space Cutoffs Corresponding to Orbit-Limited Ion Collection in Spherical, Infinite Cylindrical and Planar Symmetries, Respectively. Results in parentheses are from Table 1 of Knott. Backscattering is not included

Surface Data for Secondary Electron Emission			Spectrum 1 "Quiet"			Spectrum 2b "Disturbed"		
			Floating Potential (volts)			Floating Potential (volts)		
Material	δ_{max}	E_{max} (eV)	3-dimen.	2-dimen.	1-dimen.	3-dimen.	2-dimen.	1-dimen.
Gold	1.45	800	-890 (-800)	-1470	-4690	-6600 (<-3000)	-11,440	-21,490
Aluminum	0.97	300	-1690 (-2150)	-26.10	-6390	-7410 (<-3000)	-12,510	-22,920
Aluminum with Oxide Coating	2.60	300	+0.49(+5) or -342 * or -1260	+0.50 or -326 * or -2100	+0.50 or -300 * or -5810	-7150 (<-3000)	-12,200	-22,560
Quartz	2.50	420	+0.37 (+5)	+0.37 or -494 * or -1570	+0.37 or -405 * or -5210	-6880 (<-3000)	-11,870	-22,138
Aquadag	0.75	350	-1700 (-2140)	-2620	-6400	-7410 (<-3000)	-12,510	-22,920
Beryllium Copper	2.20	300	+0.33(+5) or -228 * or -1390	+0.33 or -223 * or -2250	+0.33 or -211 * or -5960	-7220 (<-3000)	-12,280	-22,650
Beryllium Copper Activated	5.00	400	+1.1 (+5)	+1.1	+1.1	+0.04(+5) or -280 * or -6180	+0.17 or -278 * or -11,010	-0.17 or -275 * or -21,200
No Secondary Electrons	—	—	-1870	-2840	-6690	-7550	-12,690	-23,130

*Unstable

evidence that spacecraft geometry and sheath potential shape are important influences in determining floating potentials. It is important to natc that as floating potential becomes marc negative, It also becomes more sensitive tu tho presence of small amounts of high-energy oloctronn. Thls means that if n spacecraft should encounter conditions that are "more disturbed" than those given by Knott's spectrum 2b, the values in Table 1 meal likely tu bo significantly exceeded are those for the one-dimensional cutoff. This implies that for design purposes in whlch worst-case information is desired, it is important to do calculations with th· "most disturbed" electron spectra available.

In obtaining these results, We havc made no attempt to calculate the time needed to approach the steady-state conditions which they represent. In general, thé most negative potentials correspond to a balance between the smallest currents, and will therefore involve the longest charging times.

Also evident in Table 1 are situations in whlch the current-voltage characteristic of the surface has three roots. For these to occur, it is necessary that δ_{max} be substantially greater than one, and that the incident spectrum contain e sufficient proportion of electrons in the energy range where secondary emission is a maximum. The center root never represents a possible floating potential, because it is "unstable" in the sense that a small change in surface potential would cause a net current collection of a sign which would drive the surface potential away From this root to one on either side. A further consequence of such a situation is discussed below.

Table 2 includes the further addition of backscattered electron flux (Section 2) and therefore represents a more realistic physical situation. In most cases, the net effect of backscatter is a moderate reduction of negative floating potentials. In some cases, the reduction is large, as in the case of a gold surface exposed to the "quiet" spectrum. In several other ca. es, all associated with the quiet spectrum, backscattering changes a multiple-roc' to a single-root situation. As indicated in Section 2, we have probably underestimated backscattered fluxes, and we have also (Section 1) ignored secondary electron emission caused by ion impacts. Both of these effects would tend to Further reduce negattve potentials. However, such changes are likely to be small. The results in Table 2 should probably be regarded as consistent with observations of po.entials reaching - 19 kV on the ATS-6 spececraft, ad reported by Whipple,[17]

C-5

Table 2. Floating Potentials of Shaded Surfaces of Synchronous-Altitude Spacecraft, Using the Same Surface Properties & Incident Spectra as Assumed by Knott,[1] with Three, Two-, and One-Dimensional Velocity Space Cutoffs Corresponding to Orbit-Limited Ion Collection in Spherical, Infinite Cylindrical and Planar Symmetries, Respectively. Electron backscattering is included

Surface Data for Backscattered Electron Emission:		Spectrum 1 "Quiet"			Spectrum 2b "Disturbed"		
	Emission Coefficient η (5000 eV) Sternglass[14]	Floating Potential (volts)			Floating Potential (volts)		
Material		3-dimen.	2-dimen.	1-dimen.	3-dimen.	2-dimen.	1-dimen.
Gold	0.42	-28.0	-2k1	-28.6	-3570	-6520	-15,450
Aluminum	0.16	-1370	-2060	-5180	-6610	-11,250	-21,570
Aluminum with Oxide Coating	0.18	+0.68	+0.68 or -723 * or -1010	+0.68 or -490 * or -4210	-6200	-10,690	-20,920
Quartz	0.18	+0.55	+0.55	+0.55 or -922 * or -3190	-5860	-10,240	-20,380
Aquadag	0.08	-1560	-2390	-5900	-7090	-12,010	-22,350
Beryllium Copper	0.31	+0.64	+0.64	+0.64 or -522 * or -3420	-5710	-9870	-19,830
Beryllium Copper Activated	0.33	+1.4	+1.4	+1.4	+0.41 or -908 * or -3810	+0.54 or -843 * or -7520	+0.54 or -776 * or -17,580
No Second — or Backscattered Electrons	—	-1870.	-2840	-6.690	-7558	-12,690	-23,130

*Unstable

Figures 3-7 show current-voltage characteristics for some of the situations in Tables 1 and 2. Figure 3 shows a "typical" single-root situation in which secondary and backscatter contributions do not change the general shape of the net curtent Curve. Figure 4 shows the above-mentiorled case bf gold exposed to the quiet spectrum, in which the backscatter contribution changes a large predicted negative floating potential to a much smaller value. Figure 5 shows a triple-rbot situation. Figure 6 shows the disappearance of a triple-root situation because of backscatter. In Figure 7, secondary electron current is sufficient by itself to prohibit a negative floating potential.

We now examine situations which may arise in the case of spacecraft Which have shaded cavities containing electrically isolated interior surfaces. Figure 8 shows an idealization of such a spacecraft. We wish to show that the effects of surface concavity may cause ion dollection to be reduced more than net electron collection at an interior point such as B, relative to an exterior point A; such a situation wculd result in floating potentials more negative than those of Table 2. *Tb* demonstrate this possibility, we first note that in the presence of an isotropic ambient plasma, incident fluxes to any surface depend only[3] on the locations, in velocity space, of the cutoff boundaries inside of which the orbits of ambieht particles can conhect "Prom infinity" to the surface. Figure 8 shows aset a€the associated "cutoff orbits." We see from Figure 8 that the included angle between cutoff orbits has beeh reduced in gbing from A to B for ions but not for electrons, for Which orbits tangential to the surface are shown as reaching both A and B. Accordingly, the incident ion current contribution for the energy shown will also be reduced, but the electron contribution will not. This picture is invalid for higher-energy electrons at B, whose orbits are straighter and will have a greater tendency to connect back to the interior surfaces of the cavity. Even thbugh such higher-energy orbits will generally have lower populations than lower-energy orbits, it is not clear whether the relative current reduction at B will be greater for ions or for electrons, Hbwever, this argument is intended to demonstrate only the possibility that the bounds in Table 2 will be exceeded. On the other hand, this possibility Will be enhanced by the effects of secondary and backscattered electrons, which will tend to be recollected inside any cavity, rather than escaping into space, thus tending to increase net electron collection and driving floating potentials more negative. This effect will be strongest for backscattered electrons because their: higher emission energies Will cause them tb have straighter orbits. To draw firm donclusions will require detailed numerical simulation. An additional feature of cavities is their generally higher outgassing pressures, which will increase any tendencies for arcing tb occur. More negative flbating potentials may alsb result if the ambient electron distribution contains beam-like Constituents[18] which happen

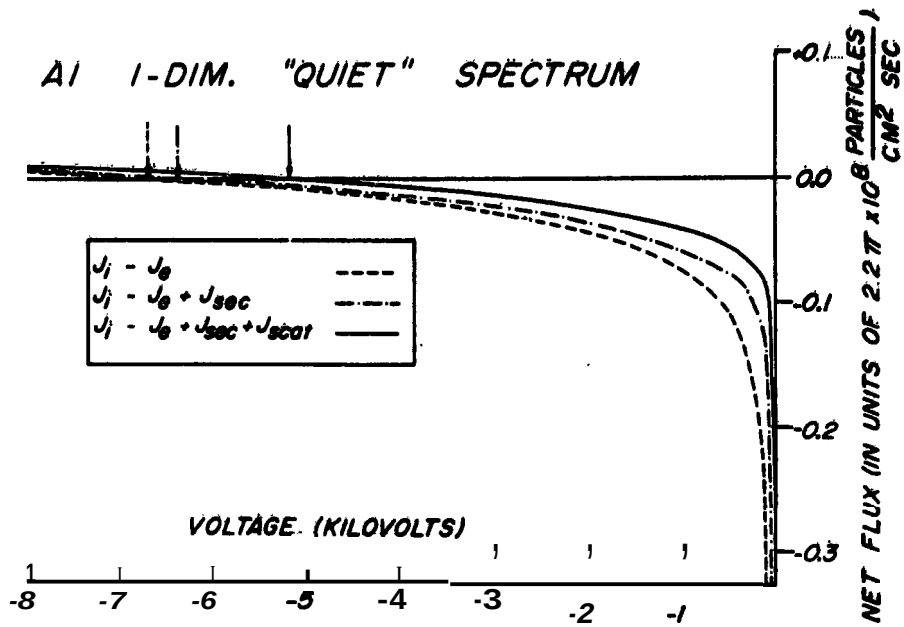

Figure 3. Current-Voltage Characteristic for Aluininum in "Quiet" Conditions, with a One-Dimensional Velocity-Space Cutoff. In Figures 3-7, the zeros of the characteristics are indicated by arrows

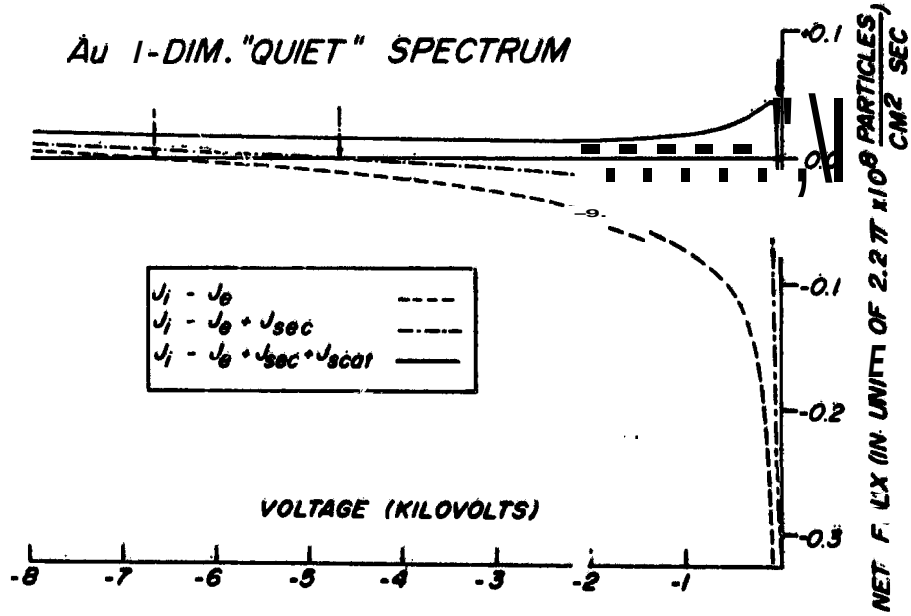

Figtire 4. Current-Voltage Characteristic for Gold in "Quiet" Conditions, with a One-Dimensional Velocity-Space Cutoff

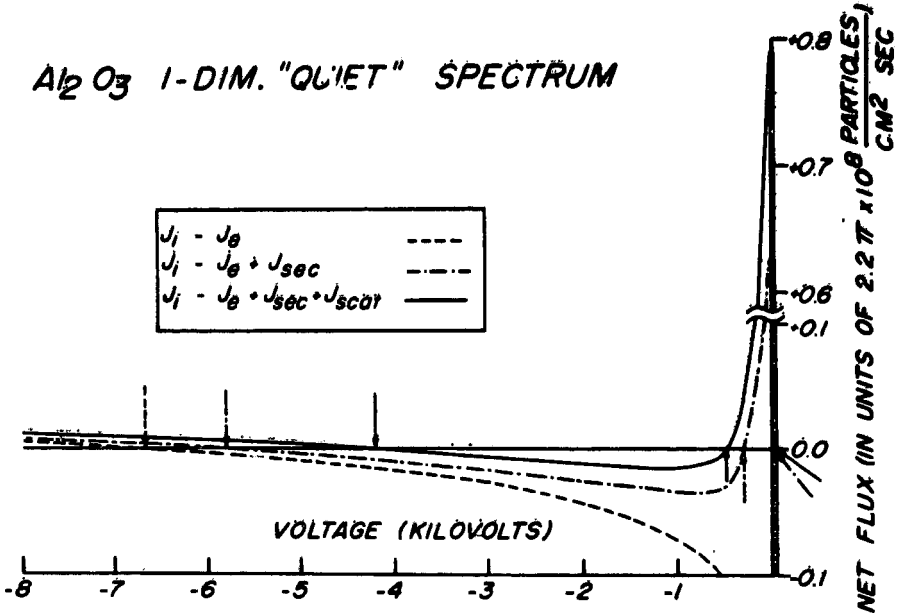

Figure 5. Cuprent-Voltage Characteristic *for* Aluminum Oxide in "Quiet" Conditions, with a Ohe-Dimensional Velocity-Space Cutoff

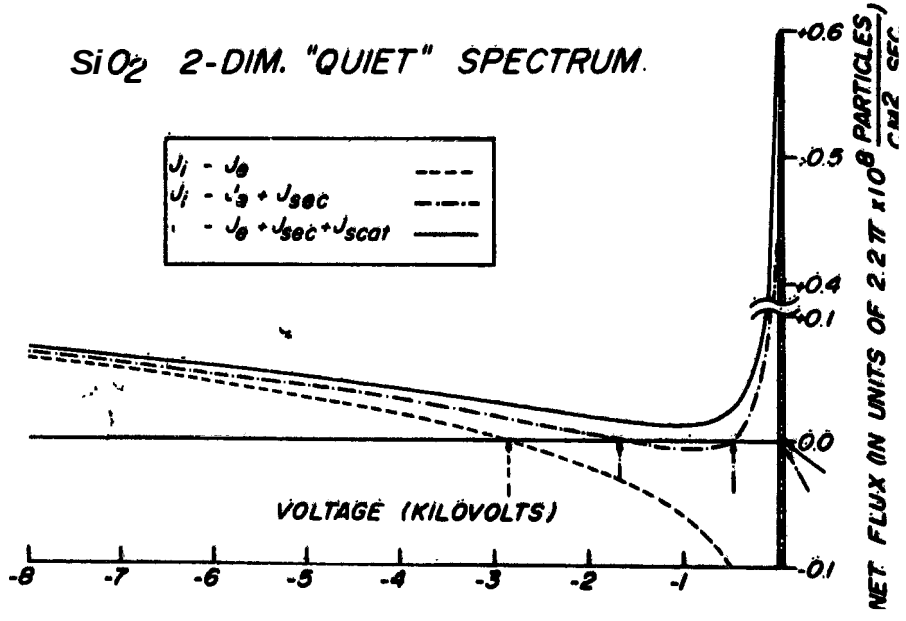

Figure 6. Current-Voltage Characteristic for Quartz in "Quiet" Conditions, with a Two-Dimensional Velocity-Space Cutoff

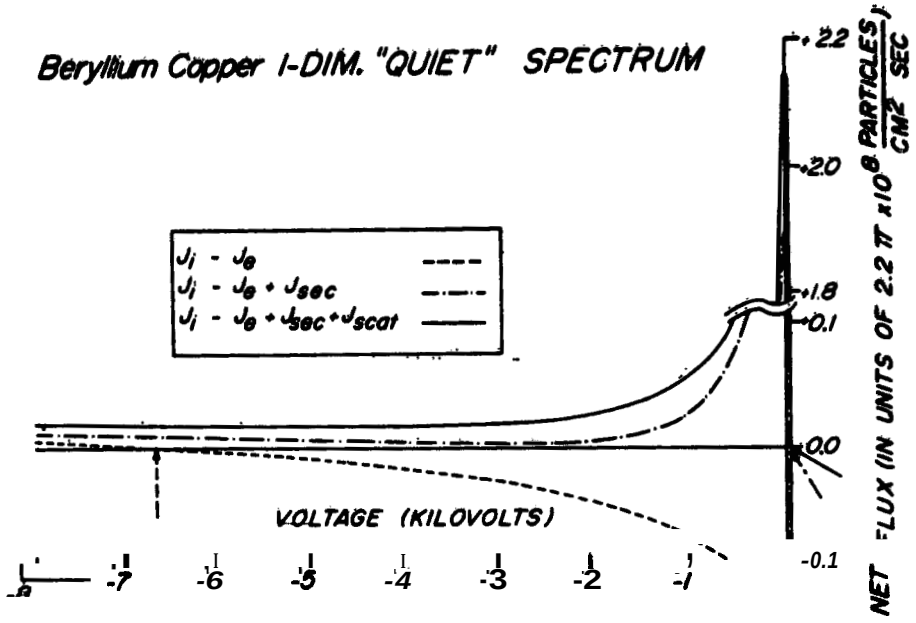

Figure 7. Current-Voltage Characteristic for Beryllium-Copper in "Quiet" Conditions, with a One-Dimensional Velocity-Space Cutoff

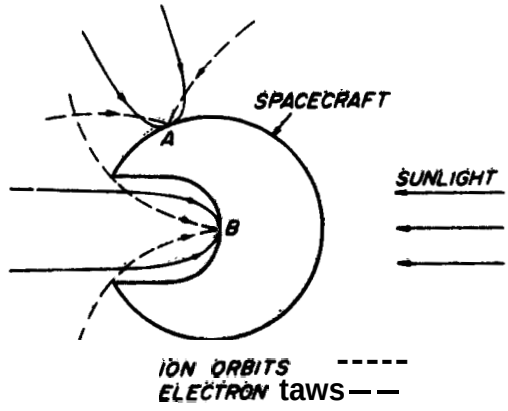

Figure 6. Spacecraft with Shaded Isolated Cavity, Showing Incident Ion and Electron Orbits with Energies Close to the Lowest For which Collection of Each Species is Possible. The orbits shown are cutoff orbits, defined as the most nearly tangential orbits for which incident particles of a given energy are able to reach a given point on the spacecraft surface, having tangential velocity component in a given direction

to be directed into a cavity. Especially severe arcing problems are known to have occurred between electronic components mounted inside a cavity at one end af the DSCS spacecraft.

Fihally, we discuss some further implications of the multiple-root results shown in Tables 1 and 2 and Figure 5. Consider a situation involving two or more adjacent but isolated spacecraft surfaces Which are made of the same material, and whose external conditions change with time, as in-the case of time-varying ambient distributions, or a dpacecraft rotation which carries these surfaces from sunlight into shadow. Such a situation might involve the continuous evolution of a single-root into a multiple-root situation, and the possibility would then arise of a "bifurcation" phenomenon in which different surface elements followed different potential histories, with a correspondingly large potential difference arising between them. Again, detailed numerical simulations are necessary in order to find out if such phenomena can actbally occur.

4. CONCLUSIONS

Upper bounds have been calculated for negative floating potentials which may be Acquired by electrically isolated shaded surfaces on synchronous spacecraft. Effects of spacecraft shape and sheath potential profile have been shown to Have large influences on such potentials. Inclusion of electroh backscattering currents causes only a moderate reduction of these negative potentials in mast cases. For isolated surfaces inside shaded cavities, negative floating potentials may exceed thoee on convex surfaces. In some conditions, two possible floating potentials exist, leading to the possibility of "bifurcation phenomena" in which adjacent isolated surfaces made of the same material may follow different charging histories.

Acknowledgments

We are indebted to H. Cohen and Jen-Shih Chang for valuable comments. This work wad supported by the U. S. Air Force Office of Scientific Research under grant number AFOSR-76-2962.

References

1. Knott, K. (1972) The equilibrium potential of a magnetospheric satellite in an eclipse situation, Planet. Space Sci. 20:1137-1146.
2. Mott-Smith, H., Jr., and Langmuir, I. (1926) The theory of collectors in gaseous discharges, Phys. Rev. 28:727-760.
3. Laframboise, J. G., and Parker, L. W. (1973) Probe design for orbit-limited current cbllection, Phys. Fluids 16:629-636.
4. Bernstein, I. B., and Rabinowitz, I. N. (1959) Theory of electrostatic probes in a low-density plasma, Phys. Fluids 2:112-121.
5. Laframboise, J. G. (1966) Theory of spherical and cylindrical Langmuir probed in a collisionless, Maxwellian plasma at rest, Univ. of Toronto, Institute for Aerospace Studies, Rep. 100.
6. Fahleson, U. (1973) Plasma-vehicle interactions in Space! Some aspects of preeent knowledge and future development. In: Photon and Particle Interactions with Surfaces in Space, R. J. L. Grard, Editor,. D. Reidel Pub. Co., Dordrecht, Holland, pp. 563-569.
7. Shield, M. A., and Frank, L.A. (1970) Electron bbservations between the inner edge of the plasma sheet and the magnetosphere, J. Geophys. Res. 75:5401-5414.
8. DeForest, S.E., and McIlwain, C. E. (1971) Plasma clouds in the magnetosphere, J. Geop . Red. 76:6587-3611.
9. Polychronopulos, B. (1973) Effects of nonMaxwellian electron energy didtributions on the orbital limited current-voltage characteristics of cylindrical and spherical Langmuir prbbes under collisionless condttions. Plhsma Phys. 15:37-48.
10. Sternglass, E. J. (1950) Secondary electron emission and atomic shell structure, Phys. Rev. 80:925-926.
11. Gibbons, D. J. (1966) Secondary electran emission. In: Handbook of Vacuum Physics, A.H. Beck, Ed., Pergamon Press, Oxford, Vol. 2, pp. 301-395.
12. Hachenberg, O., and Brauer, W. (1959) Secondary electron emission from dolidd, Adv. Electrantcs EleCtron Phys. 11:413-499.
13. Sternglass, E. J. (1954) Backscattering of kilovolt electroils from solids, Phys. Rev. 95:345-358.
14. Thomas, S, and Pattinson, E. B. (1970) Range of electrons and contribution of back-scattered electrons in secondary production in aluminum, J. Phys. D: Appl. Phys. 3 :349-357.

15. Darlington, E. H., and Cosslett, V. E. (1972) Backscattering of 0.5-10 keV electrons from solid targets, J. Phys. D: Appl. Phys. 5:1969-1981.

16. Chung, M. S., and Everhart, T. E. (1974) Simple calculation of energy distribution of low-energy secondary electrons emitted from metals Under electron bombardment, J. Appl. Phys. 45:707-709.

17. Whipple, E. C., Jr. (1976) Modelling of spacecraft charging, Paper II-1, USAF-NASA Spacecraft Charging Technology Conference, Colorado Springs.

18. DeForest, S. E. (1976) The plasma environment at geosynchronous altitude, Paper I-1, USAF-NASA Spacecraft Charging Technology Conference, Colorado Springs.